J. Fluid Mech. (2007), *vol.* 588, *pp.* 59–74.
doi:10.1017/S0022112007007422 Printed in the United Kingdom

On the compressible Taylor–Couette problem

A. MANELA[1] AND I. FRANKEL[2]

[1]Department of Mathematics, Massachusetts Institute of Technology, 77 Massachusetts Avenue, Cambridge, MA 02139, USA

[2]Faculty of Aerospace Engineering, Technion – Israel Institute of Technology, Haifa 32000, Israel

(Received 11 October 2006 and in revised form 13 May 2007)

We consider the linear temporal stability of a Couette flow of a Maxwell gas within the gap between a rotating inner cylinder and a concentric stationary outer cylinder both maintained at the same temperature. The neutral curve is obtained for arbitrary Mach (*Ma*) and arbitrarily small Knudsen (*Kn*) numbers by use of a 'slip-flow' continuum model and is verified via comparison to direct simulation Monte Carlo results. At subsonic rotation speeds we find, for the radial ratios considered here, that the neutral curve nearly coincides with the constant-Reynolds-number curve pertaining to the critical value for the onset of instability in the corresponding incompressible-flow problem. With increasing Mach number, transition is deferred to larger Reynolds numbers. It is remarkable that for a fixed Reynolds number, instability is always eventually suppressed beyond some supersonic rotation speed. To clarify this we examine the variation with increasing *Ma* of the reference Couette flow and analyse the narrow-gap limit of the compressible TC problem. The results of these suggest that, as in the incompressible problem, the onset of instability at supersonic speeds is still essentially determined through the balance of inertial and viscous-dissipative effects. Suppression of instability is brought about by increased rates of dissipation associated with the elevated bulk-fluid temperatures occurring at supersonic speeds. A useful approximation is obtained for the neutral curve throughout the entire range of Mach numbers by an adaptation of the familiar incompressible stability criteria with the critical Reynolds (or Taylor) numbers now based on average fluid properties. The narrow-gap analysis further indicates that the resulting approximate neutral curve obtained in the (*Ma*, *Kn*) plane consists of two branches: (i) the subsonic part corresponding to a constant ratio Ma/Kn (i.e. a constant critical Reynolds number) and (ii) a supersonic branch which at large *Ma* values corresponds to a constant product $Ma\,Kn$. Finally, our analysis helps to resolve some conflicting views in the literature regarding apparently destabilizing compressibility effects.

1. Introduction

The Taylor–Couette (TC) instability in a fluid between rotating concentric cylinders giving rise to a secondary vortical flow ('Taylor vortices') is a classical problem in hydrodynamic stability theory (Chandrasekhar 1961; Drazin & Reid 1981; Koschmieder 1993). The problem has been investigated extensively for incompressible fluids. Rayleigh (1916) formulated a stability criterion for the mean viscous flow which is based on the inviscid perturbation equations. Subsequent analyses have considered the viscous perturbation equations where transition to instability is governed by Re_c, a critical value of the Reynolds (*Re*) number, depending on the ratios of cylinders' radii and rotation speeds. Taylor (1923) studied the narrow-gap approximation. He

found that, while in this limit $Re_c \to \infty$, the transition to instability is governed by a finite critical value of the Taylor (Ta) number. Others (see Chandrasekhar 1961) have analysed the problem for arbitrary gap widths and have demonstrated that viscosity stabilizes the flow in comparison with the inviscid Rayleigh criterion.

Only a relatively few studies have so far addressed the compressible TC problem. This flow problem is governed by additional parameters, including the temperature ratio of the cylinders and the Mach (Ma) number. Kuhlthau (1960) conducted experiments with dry air to study the effects of transonic Mach numbers ($Ma \approx 1$) on the TC instability. During each set of experiments the rotation speed (Ma) was maintained constant while the average density was increased (i.e. Kn decreased). The onset of instability was identified through a sharp increase in the torque measured on the outer (stationary) cylinder. The experiments were carried out for $0.7 \lesssim Ma \lesssim 1.5$ showing an increase in the critical Knudsen number (Kn_c) with increasing Ma (see figure 2). The value of Re_c ($\propto Ma/Kn_c$) was found to be nearly the same as in the corresponding incompressible problem.

Kao & Chow (1992) assumed axisymmetric perturbations and studied the linear stability problem for the ratio of the radii of the outer and inner cylinders $R_R = R_o/R_i = 2$. Their results apparently suggested that increasing Ma had a destabilizing effect in the sense that it decreased Re_c relative to its incompressible value. Hatay *et al.* (1993) considered various parameter combinations and non-axisymmetric perturbations. Their results essentially agreed with those of Kao & Chow (1992) in that the effect of increasing Ma, which was stabilizing for narrow gaps, apparently became destabilizing for wider gaps. In both of these studies the Reynolds number was defined on the basis of the local gas density at the inner cylinder. Unlike the average density (which is determined by the total mass of fluid within the gap), the local density is not *a priori* prescribed in experiments or simulations. Furthermore, owing to the appearance of both elevated bulk-fluid temperatures and large radial pressure gradients at supersonic speeds, the local and average densities significantly differ from each other. Consequently, comparison of the critical values of the Reynolds numbers based on the local density with their incompressible counterparts may not provide an unequivocal indication of stabilizing or destabilizing effect of increasing Ma. Rather, it will be established that the effects of increasing Ma are adequately correlated and interpreted in terms of modified $Re(\overline{Re})$ and Ta ($\overline{Ta}$) numbers which are based on average fluid properties.

For sufficiently wide gaps, instability phenomena in the TC problem occur at $Re \lesssim O(10^2)$ (Chandrasekhar 1961). Both Kao and Chow (1992) and Hatay *et al.* (1993) have studied the problem for $Ma \leqslant 4$. The Knudsen number ($\propto Ma/Re$) corresponding to the upper end is $Kn \sim O(10^{-1})$. Thus, the very use of the continuum approach may not be consistent (Cercignani 2000). Furthermore, with the advent of microfluidic systems (e.g. micro-gas turbines; see Epstein 2004), the TC problem in rarefied gases have attracted considerable interest in recent years. The axisymmetric problem has principally been studied by means of the direct simulation Monte Carlo (DSMC) method (Bird 1994). The numerical simulations follow the evolution of the system through its terminal state which, in turn, serves to classify the system response as stable or unstable. Riechelmann & Nanbu (1993) studied the problem for a Maxwell gas. They justified their application of DSMC to this problem by demonstrating a close agreement with the experimental results of Kuhlthau (1960). Stefanov & Cercignani (1993) considered the problem for a hard-sphere gas and found that, contrary to the above-mentioned claims of Kao & Chow (1992) and Hatay *et al.* (1993), increasing Ma had a stabilizing effect for $R_R = 2$. Stefanov & Cercignani (1993)

related this disagreement to the effects of rarefaction which were not considered by the former authors. They also pointed out the potential usefulness of a stability analysis based on the 'slip-flow' continuum model. Golshtein & Elperin (1995) and Usami (1995) carried out DSMC calculations for parameter combinations within the instability domain and studied the form of vortices obtained. Bird (1998) investigated the time evolution of the vortices and presented results of three-dimensional DSMC calculations. Aoki, Sone & Yoshimoto (1999) and Yoshida & Aoki (2005) applied the DSMC method to study the influence on the neutral curve of varying both temperature and velocity ratios.

All of the above-mentioned DSMC studies demonstrate that TC instability is a small $O(10^{-2})$ Knudsen phenomenon. However, the artificial 'noise' inherent in these simulations makes it difficult to identify and characterize the final states clearly, particularly for parameter combinations in the vicinity of the transition to instability. Furthermore, these simulations become extremely time-consuming in the continuum limit, obstructing accurate delineation of the domain of instability. Consequently, explicit results in the literature have been presented only for a limited number of parameter combinations.

Recently, Yoshida & Aoki (2006) have studied the corresponding linear stability problem based on the Bhatnagar–Gross–Krook (BGK) model of the Boltzmann equation for $R_R = 2$. A close agreement was found with continuum Navier–Stokes calculations. The present contribution is intended to complement the above studies by considering the corresponding linear hydrodynamic temporal stability problem based on the Navier–Stokes 'slip-flow' continuum model for (arbitrarily) small Knudsen numbers. Our main objective is to gain some insight into the physical mechanism causing suppression of the TC instability at moderately large supersonic speeds of rotation. In § 2 we formulate the general problem for a perfect monatomic Maxwell gas. In § 3 the viscous-compressible reference Couette flow is studied. The linear stability analysis is presented in § 4 and the narrow-gap limit is discussed in § 5. Finally, some concluding remarks are given in § 6. For convenient reference the formulations of the linearized perturbation problems are explicitly presented in the Appendices.

2. Formulation of the problem

We consider a perfect monatomic Maxwell gas confined between concentric cylinders which are maintained at the same uniform temperature T_i. The gap width between the cylinders is ΔR. The inner cylinder is rotating with an angular rate Ω_i while the outer is kept stationary. To render the problem dimensionless we normalize the position vector by R_i, the velocity vector by $U_i = \Omega_i R_i$, gas density by its mean value ρ_{av} (associated with the total mass of the gas within the gap), the temperature by T_i and the pressure by $\rho_{av} R T_i$ (wherein R denotes the gas constant). The shear viscosity and heat conductivity are normalized by μ_i and κ_i, their respective values at T_i. The resulting dimensionless problem is governed by the continuity equation

$$\frac{\partial \rho}{\partial t} + \nabla \cdot (\rho \boldsymbol{u}) = 0, \tag{2.1}$$

momentum equation

$$\rho \frac{\mathrm{D}\boldsymbol{u}}{\mathrm{D}t} = -\frac{1}{\gamma Ma^2} \nabla p + \frac{\Delta R}{R_i} \frac{1}{Re} \nabla \cdot \boldsymbol{p}, \tag{2.2}$$

and energy equation

$$\rho\frac{\mathrm{D}T}{\mathrm{D}t}=-\frac{\Delta R}{R_i}\frac{\gamma}{Pr\,Re}\nabla\cdot\boldsymbol{q}-(\gamma-1)p\nabla\cdot\boldsymbol{u}+\gamma(\gamma-1)\frac{\Delta R}{R_i}\frac{Ma^2}{Re}\Phi, \tag{2.3}$$

as well as the perfect gas equation of state

$$p=\rho T. \tag{2.4}$$

In the above,

$$\boldsymbol{p}=\mu\left[\nabla\boldsymbol{u}+(\nabla\boldsymbol{u})^{\dagger}-\tfrac{2}{3}\nabla\cdot\boldsymbol{u}\boldsymbol{I}\right] \tag{2.5}$$

is the Newtonian deviatoric stress,

$$\boldsymbol{q}=-\kappa\nabla T \tag{2.6}$$

is the heat flux density satisfying the Fourier law and $\Phi=\boldsymbol{p}:\nabla\boldsymbol{u}$ is the rate of dissipation. Also appearing above are the parameters $Re=\rho_{av}U_i\Delta R/\mu_i$, the Reynolds number, $Ma=U_i/(\gamma RT_i)^{1/2}$, the Mach number (with $\gamma=c_p/c_v$ denoting the ratio of the specific heats at constant pressure and volume, respectively), and the Prandtl number $Pr=\mu_i c_p/\kappa_i$. For a Maxwell gas $\gamma=5/3$, $Pr=2/3$ and

$$\mu,\kappa=T \tag{2.7}$$

(Chapman & Cowling 1970). The above equations are supplemented by a normalization condition on the density, $\bar{\rho}=1$ (see (3.1)), and boundary conditions imposing the vanishing of the normal velocity and specifying the velocity slip and temperature jump at the walls. Employing a cylindrical coordinate system (r,θ,z), where z coincides with the common axis of symmetry, and denoting by (U,V,W) the corresponding components of $\boldsymbol{u}$, these boundary conditions are explicitly

$$U=0,\ V=\begin{bmatrix}1\\0\end{bmatrix}\pm\zeta\left(\frac{\partial V}{\partial r}-\frac{V}{r}\right),\ W=\pm\zeta\frac{\partial W}{\partial r},\ T=1\pm\tau\frac{\partial T}{\partial r}\ \text{at}\ r=\begin{bmatrix}1\\R_R\end{bmatrix} \tag{2.8}$$

(Sone 2002). In (2.8) we make use of $\zeta=1.1466(\Delta R/R_i)Kn'$ and $\tau=2.1904(\Delta R/R_i)Kn'$ (as obtained by Albertoni, Cercignani & Gotusso 1963 for the BGK model), wherein Kn' denotes the Knudsen number, the ratio of the mean free path, based on the average density and temperature (see (3.1)), and the gap width, ΔR. For a Maxwell gas, using the prevailing variable hard-sphere model (Bird 1981),

$$Kn'=\left(\frac{10}{3\pi}\right)^{1/2}\frac{Ma}{Re}\bar{T}^{1/2}. \tag{2.9}$$

3. The reference Couette flow

The reference state is a steady cylindrical Couette flow wherein $V^{(0)}$, the azimuthal fluid speed, as well as $T^{(0)}$, $p^{(0)}$ and $\rho^{(0)}$ are only functions of the radial coordinate. Mean values of the various fields are accordingly given by

$$\bar{F}=\frac{1}{\pi\left(R_R^2-1\right)}\int_1^{R_R}F^{(0)}r\,\mathrm{d}r. \tag{3.1}$$

For this flow $\nabla\cdot\boldsymbol{U}^{(0)}\equiv 0$ and the equation of continuity (2.1) is trivially satisfied for all Ma. From the azimuthal θ-component of the equation of motion we obtain

$$\frac{\mathrm{d}}{\mathrm{d}r}\left(r^2p_{r\theta}^{(0)}\right)=0 \tag{3.2}$$

for the $r\theta$-component of the deviatoric stress

$$p_{r\theta}^{(0)} = \mu^{(0)} r \frac{\mathrm{d}}{\mathrm{d}r}\left(\frac{V^{(0)}}{r}\right). \tag{3.3}$$

The former equation is readily integrated to yield

$$p_{r\theta}^{(0)} = \frac{A}{r^2}, \tag{3.4}$$

where the constant A is to be determined subsequently from the boundary conditions (2.8). Substituting (3.4) into (2.3) leads to

$$T^{(0)} \frac{\mathrm{d}}{\mathrm{d}r}\left(T^{(0)} r \frac{\mathrm{d}T^{(0)}}{\mathrm{d}r}\right) + \frac{4}{9} Ma^2 A^2 r^{-3} = 0, \tag{3.5}$$

representing the balance between heat conduction and the rate of viscous dissipation. Integration of this ordinary nonlinear second-order equation together with the boundary conditions (2.8) yields in principle $T^{(0)}(r; A)$. Integration of the equation obtained by use of $T^{(0)}$ in conjunction with (2.7), (3.3) and (3.4) and the boundary conditions (2.8) then yields $V^{(0)}(r)$ and the constant A. Once $T^{(0)}(r)$ and $V^{(0)}(r)$ have been obtained, $p^{(0)}(r)$ and $\rho^{(0)}(r)$ are calculated from the radial component of the equation of motion (2.2) together with the equation of state (2.4) and the normalization condition $\bar{\rho} = 1$ (see (3.1)). This course is followed in § 5 in the narrow-gap limit. For an arbitrary gap width, $T^{(0)}(r)$ and $V^{(0)}(r)$ (and subsequently $\rho^{(0)}(r)$ and $p^{(0)}(r)$) have been computed by means of MATLAB routines.

Figure 1 describes the effects of increasing Mach number on the radial distribution of temperature and velocity in the steady Couette flow for $R_R = 1.12$, $Kn = 0.014$ and the indicated values of Ma. (Unlike Kn', associated with the average temperature, Kn is based on the wall temperature T_i. Here and in subsequent figures we refer to the latter because it is Kn which is *a priori* specified in experiments and simulations.) The distributions of $V^{(0)}$ (lower part) and $T^{(0)}$ (upper part) are presented in terms of the shifted radial coordinate $y = (r - 1)R_i/\Delta R$. The solid lines are obtained via a numerical integration of the above continuum 'slip-flow' model. The crosses mark the corresponding distributions obtained via Monte Carlo simulations. With the exception of $T^{(0)}$ in the outer portion of the gap at the largest $Ma\,(= 7)$ presented, the two solutions nearly coincide, which lends support to the present use of the simplified continuum 'slip-flow' model. The discrepancy at $Ma = 7$ could be reduced by replacing Kn' in (2.8) with a Knudsen number based on local rather than average fluid properties. In particular, owing to centrifugal forces and the attendant radial pressure gradients, at $Ma = 7$ the local density at the outer cylinder is substantially larger than the mean, yielding a smaller local Knudsen number and hence a smaller temperature jump there. However, this modification may not be entirely consistent. Furthermore, as verified by numerical calculations, it only results in slight changes in the neutral curve, and has therefore not been pursued.

Figure 1(*a*) shows that the normalized velocity is only slightly affected by increasing the Mach number up to $Ma = 7$. This may be related to the above observation that $\nabla \cdot \boldsymbol{u}^{(0)} = 0$ for the reference Couette flow at all Ma. Furthermore, extrapolation to large Ma of the narrow-gap result (5.7) indicates a finite limit of the velocity distribution. Since for all Ma the rate of strain remains essentially bounded at $\sim U_i/\Delta R$, so does the velocity slip as well (see (2.8)).

For future reference we note that significant changes do take place in the temperature distribution. Thus, while at $Ma = 0.5$, $T^{(0)}$ is still nearly uniform at

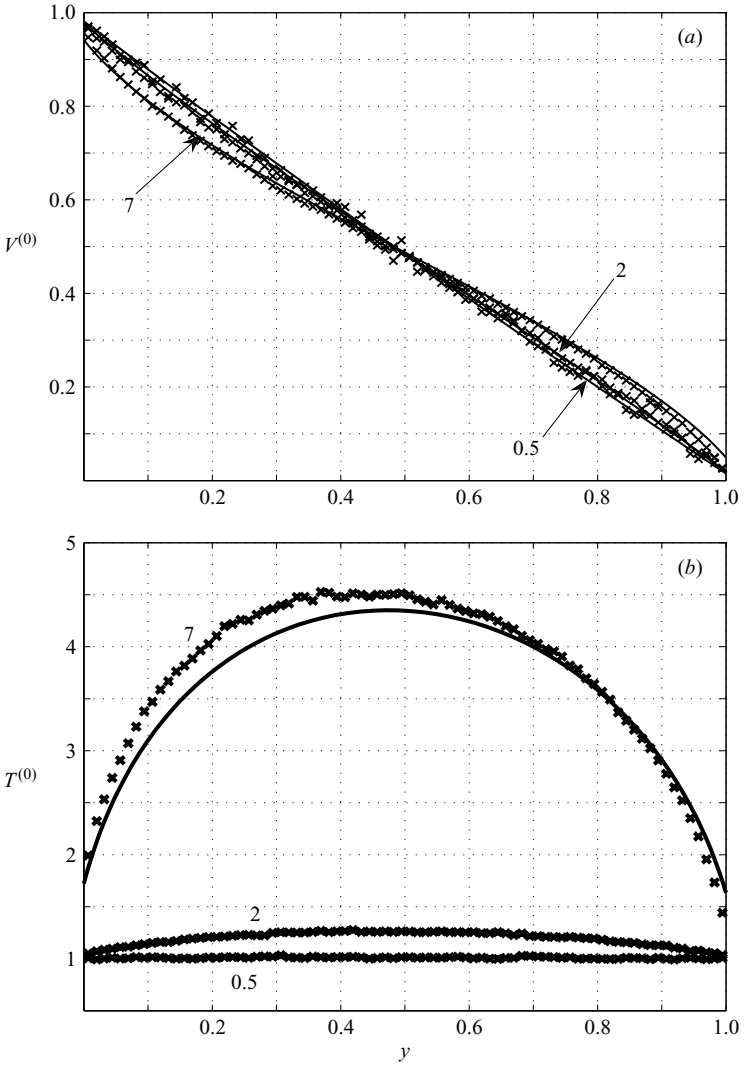

FIGURE 1. Radial distributions of (*a*) $V^{(0)}$ and (*b*) $T^{(0)}$ in the reference Couette flow for $R_R = 1.12$ and $Kn = 0.014$ at the indicated values of *Ma*. The solid lines represent the 'slip-flow' continuum model; crosses mark DSMC results.

unity (i.e. the corresponding incompressible solution), with *Ma* increasing further, $T^{(0)}$ within the bulk of the fluid, as well as the temperature jump at the walls, is rapidly increasing. This trend accords with the balance of heat conduction and rate of dissipation represented by (3.5) and reflects the rapid ($\sim Ma^6$ at large *Ma* for a narrow gap; see (5.8) *et seq.*) increase of the latter.

4. Stability analysis

The linear temporal stability analysis of the reference Couette flow is studied by assuming that it is perturbed by small spatially harmonic perturbations. Thus, the

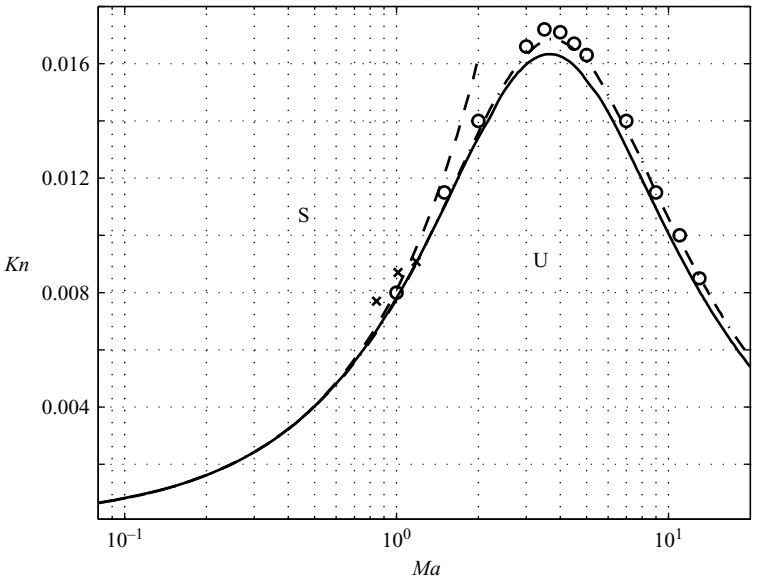

FIGURE 2. The neutral curve separating the plane of parameters (Ma, Kn) into respective domains of unstable (U), $\omega > 0$, and stable (S), $\omega < 0$, response for $R_R = 1.12$ (solid line). Also presented are the corresponding DSMC (circles) and experimental (Kuhlthau 1960, crosses) results together with the curves $Re \approx 127$ (dashed) and $\overline{Re} \approx 127$ (dash-dotted).

above-mentioned fields are generically represented by the sum

$$F(r, \theta, z, t) = F^{(0)}(r) + \phi^{(1)}(r) \exp\left[\mathrm{i}\left(\frac{R_i}{\Delta R} kz + n\theta\right) + \frac{R_i}{\Delta R}\omega t\right], \tag{4.1}$$

wherein $F^{(0)}(r)$ represents the steady reference field, the real k and integer n, respectively represent the axial- and azimuthal-perturbation wavenumbers and the complex-valued ω its growth rate. Substituting (4.1) in (2.1)–(2.8) and neglecting nonlinear terms in the perturbations, we obtain the linear homogeneous perturbation problem (Appendix A). The dispersion relation $\omega = \omega(k, n; Kn, Ma, R_R)$ is calculated by means of the Chebyshev collocation method (Peyret 2002). This method transforms the perturbation problem into an algebraic eigenvalue problem consisting of a system of $6N$ linear equations satisfied by the perturbations $\rho^{(1)}$, $u^{(1)}$, $v^{(1)}$, $w^{(1)}$, $T^{(1)}$ and $p^{(1)}$ at N discrete points across the gap. Throughout the domain of parameters corresponding to subsequent results, convergence of the calculation is established within $N < 70$. In particular, unlike DSMC computations, there is no difficulty in obtaining results for arbitrarily small $Kn > 0$.

For a stationary outer cylinder our calculations invariably yield real-valued ω. Accordingly, the onset of instability takes place via 'exchange of stabilities' (Chandrasekhar 1961), i.e. $\omega = 0$. Furthermore, in all cases examined we found that the critical mode of instability is axisymmetric, i.e. $n = 0$. We focus on $R_R = 1.12$ so as to allow for a comparison with the experimental observations of Kuhlthau (1960).

Figure 2 presents the neutral curve (solid line) separating the (Ma, Kn) plane into respective stable (S, $\omega < 0$) and unstable (U, $\omega > 0$) domains as obtained from the calculation outlined above. Also appearing in the figure are our corresponding DSMC results (circles) and the experimental observations of Kuhlthau (1960, crosses), as well

as the curves representing $Re \approx 127$ (dashed line) and $\overline{Re} = 127$ (dash-dotted; see (4.2) *et seq.*).

The stability limit in the corresponding incompressible Taylor–Couette problem is characterized by the critical Reynolds number $Re \approx 127$ and wavenumber $k_{cr} \approx 3.13$ (Chandrasekhar 1961). The latter wavenumber is obtained at the lower left part of the present stability boundary and is moderately decreasing with increasing Ma across the neutral curve to ≈ 2.88 at $Ma = 15$. Furthermore, up to $Ma \approx 1$ the present neutral curve nearly coincides with the dashed line representing $Re \approx 127$. These observations are consistent with $T^{(0)}(r)$ being nearly uniform at subsonic speeds (see figure 1). The energy equation (2.3) is thus effectively decoupled from the dynamic problem (2.1)–(2.2) and, with $\nabla \cdot \boldsymbol{u}^{(0)}$ identically vanishing, the latter becomes qualitatively similar to the corresponding incompressible problem (see § 6).

At transonic speeds ($Ma \approx 1$) we note the fair agreement between the present analysis and the experimental results of Kuhlthau (1960). The relatively small differences may be attributed to the fact that the experiments were conducted with dry air whereas the present model considers a monatomic Maxwell gas. With further increasing $Ma \gtrsim 1$ we observe the neutral curve increasingly deviating from the asymptote $Re \approx 127$ towards larger Re values. Perhaps the most remarkable feature of the present results is that the neutral curve passes through a maximum (at $Ma \approx 3.65$, $Kn \approx 0.0163$; *cf.* Yoshida & Aoki 2006). Thus, for all $Kn \lesssim 0.0163$ there exists an upper bound of Ma beyond which the system recovers its stability. Alternatively, for a given $Re \gtrsim 127$ there is a Mach number beyond which the Couette flow (which is unstable at all smaller Ma) becomes stable. To verify this result we have conducted DSMC calculations (Bird 1994). We use a rectangular computational domain in a meridional plane whose axial dimension is twice the radial gap width. At the cylindrical walls we assume purely diffuse reflection. Periodicity is imposed in the axial direction.† The stability problem is studied by considering the initial-value problem wherein the gas occupying the computational domain is initially at equilibrium characterized by the uniform density ρ_{av} and temperature T_i, and both cylinders stationary. Rotation of the inner cylinder is impulsively started at $t = 0^+$. The subsequent evolution of the flow field is followed through its terminal state. Each circle in the figure marks the largest value of Kn where instability is observed in the simulation at the corresponding Ma. The agreement between the results of the molecular nonlinear DSMC calculation of the initial-value problem and the neutral curve resulting from the linearized eigenvalue problem based on the continuum model is indeed gratifying. In particular, the occurrence of a maximum beyond which the neutral curve descends with Ma is unequivocally confirmed.

To gain some insight into this behaviour of the neutral curve we return to figure 1, which describes the reference Couette flow. Inspection of figure 2 reveals that, for $Kn = 0.014$, $Ma = 2$ and 7 correspond to the points just before entering and shortly after leaving the unstable domain, respectively. As we have already observed in figure 1, increasing Ma from 2 to 7 predominantly results in elevated gas temperatures accompanied by only a relatively small modification of the reference velocity

† For the assumed aspect ratio of the computational domain, this condition corresponds to the discrete spectrum $k = n\pi$ ($n = 1, 2, \ldots$) of perturbation wavenumbers (Manela & Frankel 2005). We have verified that the location of the neutral curve is rather insensitive to the exact value of the critical wavenumber. The basic harmonic of the discrete spectrum thus adequately approximates the above-mentioned $2.88 \lesssim k_{cr} \lesssim 3.13$ (which points to the existence of an 'adaptation' mechanism of the compressible flow).

distribution. This seems to suggest that, as in the corresponding incompressible problem, stability is essentially determined through a balance between destabilizing inertial effects and retarding viscous effects. Such a balance is expressible in terms of a critical Reynolds number. However, one needs to consider that, owing to the elevated temperatures at supersonic speeds, bulk-fluid density and viscosity vary considerably across the fluid. To account roughly for these we introduce

$$\overline{Re} = \frac{U_i \Delta R}{\bar{\nu}}$$

based on $\bar{\nu}$, the mean kinematic viscosity in the reference state. Comparison with (2.9) yields

$$\overline{Re} = \left(\frac{10}{3\pi}\right)^{1/2} \frac{Ma}{Kn} \overline{\left(\frac{T^{(0)}}{\rho^{(0)}}\right)}^{-1}, \tag{4.2}$$

where use is made of (2.7). As mentioned above, the dash-dotted curve in the figure represents $\overline{Re} \approx 127$. At subsonic speeds, $Ma \lesssim 1$, the ratio $T^{(0)}/\rho^{(0)}$ is nearly uniform throughout the gap and this curve accordingly coincides with the dashed line $Re \approx 127$. At supersonic speeds $\overline{T^{(0)}/\rho^{(0)}}$ increases faster than linearly with Ma (*cf.* (5.14)). Consequently, in order to maintain a constant value of $\overline{Re}$, Kn needs to diminish with increasing Ma. Thus, the appearance of the descending branch of the neutral curve is related to increased dissipation rates at supersonic speeds. The figure demonstrates that $\overline{Re} \approx 127$ is indeed a surprisingly close approximation of the neutral curve. To gain further insight into the behaviour at supersonic speeds we consider in the next section the narrow-gap limit of the present problem.

5. The narrow-gap limit

We consider the limit $\Delta R/R_i = \epsilon \to 0$ and use the above-defined shifted radial coordinate y:

$$r = 1 + \epsilon y. \tag{5.1}$$

Since $V^{(0)}$ undergoes an $O(1)$ change across the narrow gap, we anticipate that $p_{r\theta}^{(0)} \sim O(\epsilon^{-1})$ (see (3.3)), and thus select in (3.4) $A = A_0/\epsilon$. Assuming that, for $\epsilon \to 0$, $T^{(0)} \sim T_0^{(0)} + o(1)$, we obtain from (3.5)

$$T_0^{(0)} \frac{\mathrm{d}}{\mathrm{d}y}\left(T_0^{(0)} \frac{\mathrm{d}T_0^{(0)}}{\mathrm{d}y}\right) + \frac{4}{9} Ma^2 A_0^2 = 0. \tag{5.2}$$

Furthermore, it is subsequently established that a consistent limit process of the stability problem requires that $Kn \sim \epsilon^{1/2}$ (see (5.11)). Thus, to leading order in ϵ, (5.2) is supplemented with the boundary conditions

$$T_0^{(0)} = 1 \quad \text{at} \quad y = 0, 1. \tag{5.3}$$

From (5.2) one readily verifies that $T_0^{(0)}$ is convex, possessing a single maximum $T_0^{(0)} = T_m$ at $y = y_m$. Integrating twice while making use of (5.3) yields

$$y = \frac{1}{2}\left[1 \mp \left(\frac{T_m - T_0^{(0)}}{T_m - 1}\right)^{1/2} \frac{2T_m + T_0^{(0)}}{2T_m + 1}\right] \tag{5.4}$$

and

$$A_0 = -\frac{2T_m + 1}{Ma}\left[2(T_m - 1)\right]^{1/2}. \tag{5.5}$$

From (3.3) together with (3.4) we have

$$\frac{\mathrm{d}V_0^{(0)}}{\mathrm{d}y} = \frac{A_0}{T_0^{(0)}}, \tag{5.6}$$

hence $V_0^{(0)}$ is monotonically decreasing and antisymmetric relative to $y = 1/2$. Integrating in conjunction with (5.4), (5.5) and (2.8), which effectively becomes a no-slip condition, we obtain

$$y = \frac{1}{2} - \frac{V_0^{(0)} - 1/2}{1 + Ma^2/27}\left[1 + \frac{1}{18}Ma^2 - \frac{2}{27}Ma^2\left(V_0^{(0)} - \frac{1}{2}\right)^2\right] \tag{5.7}$$

and

$$T_m = 1 + \frac{1}{18}Ma^2. \tag{5.8}$$

From the radial component of the equation of motion together with (2.4) and (5.6), we obtain

$$p_0^{(0)} \sim A_0\left[1 + O(\epsilon)\right], \tag{5.9}$$

i.e. to leading order $p_0^{(0)}$ is uniform throughout the gap indicating that centrifugal forces become negligible in this limit. Furthermore, from (2.4), (5.4) and (5.7),

$$\rho_0^{(0)} = \frac{1 + Ma^2/27}{1 + 2Ma^2 V_0^{(0)}\left(1 - V_0^{(0)}\right)/9}. \tag{5.10}$$

Thus, in agreement with the uniformity of the pressure and the variation of the temperature across the gap, the density attains a minimum at the middle of the gap ($V^{(0)} = 1/2$) and is increasing towards the inner and outer cylinder walls.

From (5.2), (5.5), and (5.8) we find that (as mentioned at the conclusion of § 3) at large Ma the rate of dissipation indeed grows like Ma^6. Owing to this the temperature within the gap increases like Ma^2. In contrast, the variation with growing Ma of the monotonically diminishing fluid velocity is bounded, and thus $V^{(0)}(y; Ma)$ approaches a finite limit at large Ma.

For future reference we note that the foregoing derivation for $\epsilon \to 0$ with Ma fixed may become non-uniform at large Ma. Thus, from (5.4) in conjunction with (5.11) we find that the temperature jump at the walls becomes non-negligible when $\epsilon^{1/2}Ma^4 \sim 1$. Similarly, further increasing Ma, when $\epsilon^{1/2}Ma^2 \sim 1$, the velocity slip and the radial pressure gradient at the inner cylinder both become significant. Numerical calculations at large $Ma\,(= 7)$ and diminishing ϵ confirm that the convergence of $p^{(0)}$ and $V^{(0)}$ to the above narrow-gap limit is indeed faster than that of $T^{(0)}$. Furthermore, owing to the diminishing temperature jump for $\epsilon \to 0$, these calculations show that $T^{(0)}(r; Ma, \epsilon)$ approaches the narrow-gap limit from above.

We now turn to identify the limit process appropriate to the stability analysis for fixed Ma when $\epsilon \to 0$. In the corresponding incompressible-flow problem (for a stationary outer cylinder) the Taylor number approaches the constant limit

$$Ta = \frac{4\Omega_i^2(\Delta R)^4}{\left(R_R^2 - 1\right)\nu^2} \approx 3390$$

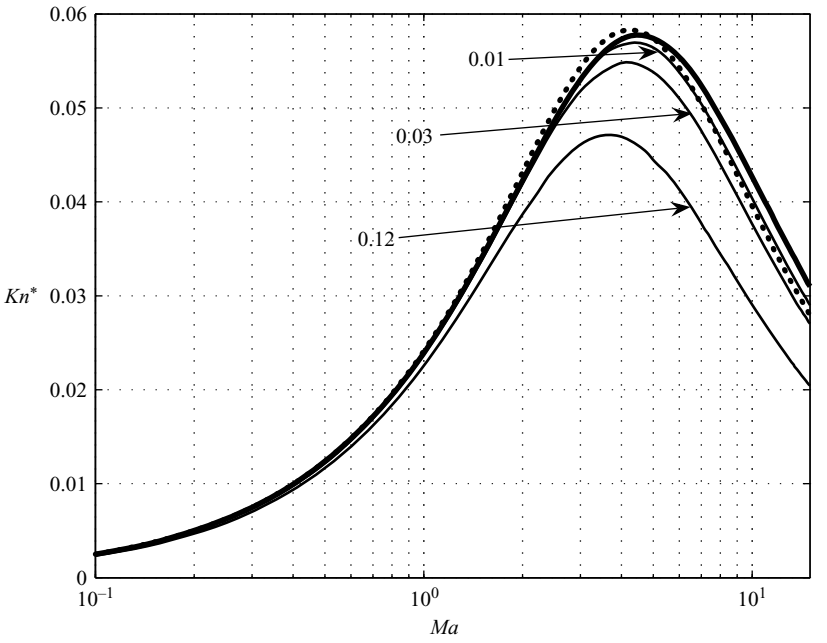

FIGURE 3. The neutral curve in the compressible narrow-gap limit $\epsilon \to 0$. The solid lines correspond to the exact numerical solution at the indicated values of ϵ. The bold solid line marks the limit $\epsilon \to 0$. The bold dotted curve describes the line $\overline{Ta} \approx 3390$.

(Drazin & Reid 1981). In the present notation $Ta \sim 2Re^2\epsilon$. Thus, for the results of the subsequent analysis to reduce with diminishing Ma to their incompressible counterparts, we require that

$$Re = \epsilon^{-1/2} Re^* \quad \text{and} \quad Kn = \epsilon^{1/2} Kn^*. \tag{5.11}$$

The growth rate of perturbations has been normalized above by $U_i/\Delta R$, whereas in the incompressible problem it is scaled by $\nu_i/(\Delta R)^2$. Hence, consistency with (5.11) requires

$$\omega = \epsilon^{1/2} \omega^*. \tag{5.12}$$

(In (5.11) and (5.12) Re^*, Kn^* and ω^* are fixed for $\epsilon \to 0$). Finally, inspection of the perturbation equations (Appendix A) reveals that a consistent limit is obtained by scaling the various perturbation amplitudes as

$$\rho^{(1)}, T^{(1)}, v^{(1)} \sim O(1)\ ;\ u^{(1)}, w^{(1)} \sim O(\epsilon^{1/2}) \quad \text{and} \quad p^{(1)} \sim \epsilon. \tag{5.13}$$

The perturbation problem thus obtained (see Appendix B) is studied by means of the Chebyshev collocation method.

Figure 3 examines convergence in the compressible narrow-gap limit $\epsilon \to 0$ when Ma is fixed. To this end we present the neutral curves ($\omega^* = 0$) in the (Ma, Kn^*) plane. The solid lines correspond to the exact problem at (finite) diminishing gap widths represented by the indicated values of ϵ ($\epsilon = 0.12$ corresponding to the neutral curve presented in figure 2). The bold solid line marks the limit $\epsilon \to 0$ and the bold dotted curve describes the line $\overline{Ta} \approx 3390$ (see (5.14) below).

All the lines presented display qualitatively similar behaviour passing through respective maxima at some intermediate supersonic speeds ($Ma \approx 3.5$–4.5) and descending thereafter. The line $\epsilon = 0.01$ nearly coincides with the limit $\epsilon \to 0$ when

$Ma \lesssim 3.5$. The relatively small discrepancy between these two curves for $Ma > 3.5$ may be related to the above-mentioned non-uniformity of the limit, in particular, the non-vanishing temperature jump at finite ϵ. This, as explained above, causes the temperature distribution to approach the narrow-gap limit from above. In agreement with the discussion preceding the introduction of $\overline{Re}$, it may thus be anticipated that the neutral curves converge to the limit $\epsilon \to 0$ from below, as indeed appears in the figure.

As mentioned above, the dash-dotted line corresponds to $\overline{Ta} \approx 3390$, where $\overline{Ta}$ is expressed by use of the relation between Ta and Re, with Re being replaced by $\overline{Re}$. To this end, we obtain from (5.6), (5.9) and (5.10) the average kinematic viscosity

$$\overline{\nu_0^{(0)}} = \left(1 + \frac{1}{27}Ma^2\right)^{-2} \left(1 + \frac{1}{9}Ma^2 + \frac{2}{405}Ma^4 + \frac{2}{25515}Ma^6\right). \tag{5.14}$$

Within the subsonic regime $Ma \lesssim 1$ (5.14) shows only a slight variation of $\overline{\nu_0^{(0)}}$ (i.e. $\overline{Re} \approx Re$). Subsequently, $\overline{\nu_0^{(0)}}$ grows nonlinearly with Ma, which requires a diminishing Kn to maintain a constant $\overline{Ta}$ ($\overline{Re}$) (*cf.* (4.2) *et seq.*). An extrapolation of (5.14) to large Mach numbers predicts that $\overline{\nu_0^{(0)}}$ grows like $\sim Ma^2$, thus the right-hand branch of the neutral curve will approximately correspond to $Ma\,Kn \approx \text{const}$.

As in figure 2, the incorporation into the 'incompressible' result of an averaged Reynolds number (intended to account for the variation with Ma of the bulk-gas properties) yields a good approximation of the neutral curve in the compressible problem. While there is obviously a certain degree of arbitrariness in selecting the specific mode of averaging fluid properties, for a narrow gap the various modes provide qualitatively and quantitatively similar approximations to the actual neutral curve.

Finally, the present results clearly confirm the stabilizing effect of increasing Ma. As demonstrated for a narrow gap in (5.10), the local fluid density at the inner (as well as outer) cylinder wall may significantly exceed the average density at supersonic speeds. For wider gaps, the radial pressure gradients associated with centrifugal forces will at supersonic speeds produce at the inner cylinder a local fluid density significantly smaller than the average. Thus, the rather questionable claim by Kao & Chow (1992) and Hatay *et al.* (1993) regarding the destabilizing role of compressibility may actually originate from a misinterpretation of their results in terms of a Reynolds number involving this local fluid density. In contrast to this, figures 2 and 3 clearly demonstrate the advantage of correlation in terms of $\overline{Re}$ and $\overline{Ta}$ which, in turn, make allowance for variation of fluid properties accompanying the elevated temperatures occurring at supersonic speeds.

6. Concluding comments

We have studied the TC problem for a Maxwell gas confined between a rotating inner cylinder and a stationary outer cylinder kept at the same temperature, focusing on the radii ratio $R_R = 1.12$ so as to allow for a comparison with the experimental results of Kuhlthau (1960). The neutral curve has been obtained through a linearized temporal stability analysis of a continuum 'slip-flow' as well as via molecular DSMC calculations of the corresponding nonlinear initial-value problem, both models yielding closely similar results. At subsonic rotation speeds the neutral curve nearly coincides with the line $Re \approx 127$, the critical value in the corresponding incompressible-flow problem. Close agreement is also obtained with Kuhlthau's measurements in the

transonic regime. With increasing $Ma \gtrsim 1$ the neutral curve deviates to increasingly larger values of Re. Furthermore, for increasing Ma at all fixed $Re > 127$, instability is eventually suppressed.

Inspection of the variation with increasing Ma of the reference Couette flow reveals the emergence of elevated bulk-fluid temperatures accompanied by only relatively modest changes in the velocity distribution (when normalized by the inner cylinder rotation speed). The latter may be attributed to the above-mentioned fact that $\boldsymbol{u}^{(0)}(r)$ trivially satisfies $\nabla \cdot \boldsymbol{u}^{(0)} = 0$ and the continuity equation at all Ma. Moreover, the inertial (Euler) portion of the equation of motion is not explicitly modified by compressibility. The elevated bulk temperatures are associated with the increasing viscous dissipation rates coupled with the dissipation–conduction balance in the energy equation. These trends are supported by the narrow-gap asymptotic results showing a limited variation with Ma of $V^{(0)}(r)$ as opposed to the bulk temperatures growing like $\sim Ma^2$.

These observations indicate that, as for the incompressible-flow TC problem, the neutral curve in the present problem essentially reflects a balance between an inertial destabilizing mechanism and a retarding effect associated with viscous dissipation. The re-stabilization at supersonic speeds thus results from increasing dissipation rates which, in turn, are substantially enhanced by the temperature dependence of the gas viscosity in combination with the elevated temperatures. The $\overline{Re} \approx 127$ and $\overline{Ta} \approx 3390$ curves presented in figures 2 and 3, respectively, roughly account for these effects.

As mentioned above, the present study has focused on $R_R \leqslant 1.12$. With increasing R_R, compressibility effects (i.e. density variations resulting from fluid motion through ambient pressure gradients) are expected to become more significant with growing centrifugal forces. According to the above observations regarding $V^{(0)}(r)$, essential elements in Rayleigh's argument carry over to the compressible-flow problem, in particular the constancy of the angular momentum (per unit mass) of a fluid element. Rayleigh's inertial mechanism may, however, be modified owing to compression accompanying fluid motion through a non-homentropic field. Further study is required to clarify these issues, which constitutes a desirable extension of the present contribution.

Appendix A. The linearized perturbation problem

To simplify notation we omit in the following the superscripts (1) in the expressions of the perturbations. The resulting perturbation problem consists of the continuity,

$$\hat{\omega}\rho + \rho^{(0)}\left(\frac{\mathrm{d}u}{\mathrm{d}r} + \frac{u}{r} + \mathrm{i}n\frac{1}{r}v + \mathrm{i}\hat{k}w\right) + \frac{\mathrm{d}\rho^{(0)}}{\mathrm{d}r}u + \mathrm{i}n\frac{V^{(0)}}{r}\rho = 0, \tag{A 1}$$

r-momentum,

$$\hat{\omega}\rho^{(0)}u + \frac{\rho^{(0)}V^{(0)}}{r}(\mathrm{i}nu - 2v) - \frac{V^{(0)2}}{r}\rho = -\frac{3}{5\gamma Ma^2}\frac{\mathrm{d}p}{\mathrm{d}r} + \frac{\Delta R}{R_i}\frac{1}{Re}\sigma_r, \tag{A 2}$$

θ-momentum,

$$\hat{\omega}\rho^{(0)}v + \frac{\rho^{(0)}V^{(0)}}{r}(\mathrm{i}nv + u) + \rho^{(0)}\frac{\mathrm{d}V^{(0)}}{\mathrm{d}r}u = -\frac{3\mathrm{i}n}{5Ma^2}\frac{1}{r}p + \frac{\Delta R}{R_i}\frac{1}{Re}\sigma_\theta, \tag{A 3}$$

z-momentum,

$$\hat{\omega}\rho^{(0)}w + \mathrm{i}n\frac{\rho^{(0)}V^{(0)}}{r}w = -\frac{3\mathrm{i}\hat{k}}{5Ma^2}p + \frac{\Delta R}{R_i}\frac{1}{Re}\sigma_z, \tag{A 4}$$

and energy,

$$\begin{aligned}\hat{\omega}\rho^{(0)}T + \mathrm{i}n\frac{\rho^{(0)}V^{(0)}}{r}T + \rho^{(0)}\frac{\mathrm{d}T^{(0)}}{\mathrm{d}r}u \\ = \frac{5\Delta R}{2R_i}\frac{1}{Re}h - \frac{2}{3}p^{(0)}\left(\frac{\mathrm{d}u}{\mathrm{d}r} + \frac{u}{r} + \mathrm{i}n\frac{1}{r}v + \mathrm{i}\hat{k}w\right) + \frac{10\Delta R}{9R_i}\frac{Ma^2}{Re}D,\end{aligned} \tag{A 5}$$

equations, together with the equation of state

$$p = \rho^{(0)}T + T^{(0)}\rho. \tag{A 6}$$

In the above, $\hat{\omega} = (R_i/\Delta R)\omega$ and $\hat{k} = (R_i/\Delta R)k$. The perturbation problem is supplemented by the boundary conditions (see (2.8))

$$u = 0,\ v = \pm\zeta\frac{\partial v}{\partial r},\ w = \pm\zeta\frac{\partial w}{\partial r},\ T = \pm\tau\frac{\partial T}{\partial r} \quad \text{at} \quad r = \begin{bmatrix}1\\ R_R\end{bmatrix}. \tag{A 7}$$

The assumed form (4.1) ensures that the normalization condition for the density perturbation (i.e. the homogeneous equivalent of (3.1)) is satisfied. In the viscous-stress terms of (A 2)–(A 4),

$$\begin{aligned}\sigma_r = {} & \frac{4}{3}T^{(0)}\frac{\mathrm{d}^2u}{\mathrm{d}r^2} + \frac{4}{3}\left(\frac{\mathrm{d}T^{(0)}}{\mathrm{d}r} + \frac{T^{(0)}}{r}\right)\frac{\mathrm{d}u}{\mathrm{d}r} - \left[\frac{2}{3r}\frac{\mathrm{d}T^{(0)}}{\mathrm{d}r} + T^{(0)}\left(\frac{4}{3r^2} + \frac{n^2}{r^2} + \hat{k}^2\right)\right]u \\ & + \frac{\mathrm{i}n}{3r}T^{(0)}\frac{\mathrm{d}v}{\mathrm{d}r} - \frac{\mathrm{i}n}{3r}\left[2\frac{\mathrm{d}T^{(0)}}{\mathrm{d}r} + 7\frac{T^{(0)}}{r}\right]v + \frac{\mathrm{i}\hat{k}}{3}T^{(0)}\frac{\mathrm{d}w}{\mathrm{d}r} - \frac{2\mathrm{i}\hat{k}}{3}\frac{\mathrm{d}T^{(0)}}{\mathrm{d}r}w \\ & + \frac{\mathrm{i}n}{r}\left[\frac{\mathrm{d}V^{(0)}}{\mathrm{d}r} - \frac{V^{(0)}}{r}\right]T,\end{aligned} \tag{A 8}$$

$$\begin{aligned}\sigma_\theta = {} & \frac{\mathrm{i}n}{3r}T^{(0)}\frac{\mathrm{d}u}{\mathrm{d}r} + \frac{\mathrm{i}n}{r}\left[\frac{\mathrm{d}T^{(0)}}{\mathrm{d}r} + \frac{7}{3r}T^{(0)}\right]u + T^{(0)}\frac{\mathrm{d}^2v}{\mathrm{d}r^2} + \left[\frac{\mathrm{d}T^{(0)}}{\mathrm{d}r} + \frac{T^{(0)}}{r}\right]\frac{\mathrm{d}v}{\mathrm{d}r} \\ & - \left[\frac{1}{r}\frac{\mathrm{d}T^{(0)}}{\mathrm{d}r} + T^{(0)}\left(\frac{4n^2}{3r^2} + \frac{1}{r^2} + \hat{k}^2\right)\right]v - \frac{n\hat{k}}{3r}T^{(0)}w + \left[\frac{\mathrm{d}V^{(0)}}{\mathrm{d}r} - \frac{V^{(0)}}{r}\right]\frac{\mathrm{d}T}{\mathrm{d}r} \\ & + \left[\frac{\mathrm{d}}{\mathrm{d}r}\left(\frac{\mathrm{d}V^{(0)}}{\mathrm{d}r} - \frac{V^{(0)}}{r}\right) + \frac{2}{r}\left(\frac{\mathrm{d}V^{(0)}}{\mathrm{d}r} - \frac{V^{(0)}}{r}\right)\right]T,\end{aligned} \tag{A 9}$$

and

$$\begin{aligned}\sigma_z = {} & \frac{\mathrm{i}\hat{k}}{3}T^{(0)}\frac{\mathrm{d}u}{\mathrm{d}r} + \mathrm{i}\hat{k}\left(\frac{\mathrm{d}T^{(0)}}{\mathrm{d}r} + \frac{1}{3}\frac{T^{(0)}}{r}\right)u - \frac{n\hat{k}}{3}\frac{T^{(0)}}{r}V + T^{(0)}\frac{\mathrm{d}^2w}{\mathrm{d}r^2} \\ & + \left(\frac{\mathrm{d}T^{(0)}}{\mathrm{d}r} + \frac{T^{(0)}}{r}\right)\frac{\mathrm{d}w}{\mathrm{d}r} - \left(n^2\frac{T^{(0)}}{r} + \frac{4\hat{k}^2}{3}T^{(0)}\right)w.\end{aligned} \tag{A 10}$$

In the heat flux and dissipation terms in (A 5),

$$h = T^{(0)}\frac{\mathrm{d}^2T}{\mathrm{d}r^2} + \left[2\frac{\mathrm{d}T^{(0)}}{\mathrm{d}r} + \frac{T^{(0)}}{r}\right]\frac{\mathrm{d}T}{\mathrm{d}r} - \left[\left(\frac{n^2}{r^2} + \hat{k}^2\right)T^{(0)} + \frac{1}{T^{(0)}}\left(\frac{\mathrm{d}T^{(0)}}{\mathrm{d}r}\right)^2\right]T \tag{A 11}$$

and

$$D = \left(\frac{\mathrm{d}V^{(0)}}{\mathrm{d}r} - \frac{V^{(0)}}{r}\right)\left[2in\frac{T^{(0)}}{r}u + 2T^{(0)}\frac{\mathrm{d}v}{\mathrm{d}r} - 2\frac{T^{(0)}}{r}v + \left(\frac{\mathrm{d}V^{(0)}}{\mathrm{d}r} - \frac{V^{(0)}}{r}\right)T\right], \quad \text{(A 12)}$$

respectively.

Appendix B. The linearized perturbation problem in the limit $\epsilon \to 0$

Substituting (5.1) together with (5.11)–(5.13) into (A 1)–(A 7), and assuming axisymmetric perturbations, yields for the leading order

$$\omega^*\rho + \rho_0^{(0)}\left(\frac{\mathrm{d}u}{\mathrm{d}y} + \mathrm{i}kw\right) + \frac{\mathrm{d}\rho_0^{(0)}}{\mathrm{d}y}u = 0, \quad \text{(B 1)}$$

$$\omega^*\rho_0^{(0)}u - 2\rho_0^{(0)}V_0^{(0)}v - V_0^{(0)2}\rho = -\frac{3}{5Ma^2}\frac{\mathrm{d}p}{\mathrm{d}y} + \frac{1}{Re^*}\sigma_y^*, \quad \text{(B 2)}$$

$$\omega^*\rho_0^{(0)}v + \rho^{(0)}\frac{\mathrm{d}V^{(0)}}{\mathrm{d}y}u = \frac{1}{Re^*}\sigma_\theta^*, \quad \text{(B 3)}$$

$$\omega^*\rho_0^{(0)}w = -\frac{3\mathrm{i}k}{5Ma^2}p + \frac{1}{Re^*}\sigma_z^*, \quad \text{(B 4)}$$

$$\omega^*\rho_0^{(0)}T + \rho_0^{(0)}\frac{\mathrm{d}T_0^{(0)}}{\mathrm{d}y}u = \frac{5}{2Re^*}h^* - \frac{2}{3}p_0^{(0)}\left(\frac{\mathrm{d}u}{\mathrm{d}y} + \mathrm{i}kw\right) + \frac{20}{9}\frac{Ma^2}{Re^*}T_0^{(0)}\frac{\mathrm{d}V_0^{(0)}}{\mathrm{d}y}\frac{\mathrm{d}v}{\mathrm{d}y}, \quad \text{(B 5)}$$

$$\rho_0^{(0)}T + T_0^{(0)}\rho = 0, \quad \text{(B 6)}$$

together with the boundary conditions

$$u = v = w = T = 0 \quad \text{at} \quad y = 0, 1. \quad \text{(B 7)}$$

The reference fields appearing in (B 2)–(B 6) are those calculated in § 5. Also appearing in (B 2)–(B 5) are

$$\sigma_y^* = \frac{4}{3}T_0^{(0)}\frac{\mathrm{d}^2u}{\mathrm{d}y^2} + \frac{4}{3}\frac{\mathrm{d}T_0^{(0)}}{\mathrm{d}y}\frac{\mathrm{d}u}{\mathrm{d}y} - k^2T_0^{(0)}u + \frac{\mathrm{i}k}{3}T_0^{(0)}\frac{\mathrm{d}w}{\mathrm{d}y} - \frac{2\mathrm{i}k}{3}\frac{\mathrm{d}T_0^{(0)}}{\mathrm{d}y}w, \quad \text{(B 8)}$$

$$\sigma_\theta^* = T_0^{(0)}\frac{\mathrm{d}^2v}{\mathrm{d}y^2} + \frac{\mathrm{d}T_0^{(0)}}{\mathrm{d}y}\frac{\mathrm{d}v}{\mathrm{d}y} - k^2T_0^{(0)}v + \frac{\mathrm{d}V_0^{(0)}}{\mathrm{d}y}\frac{\mathrm{d}T}{\mathrm{d}y} + \frac{\mathrm{d}^2V_0^{(0)}}{\mathrm{d}y^2}T, \quad \text{(B 9)}$$

$$\sigma_z^* = \frac{\mathrm{i}k}{3}T_0^{(0)}\frac{\mathrm{d}u}{\mathrm{d}y} + \mathrm{i}k\frac{\mathrm{d}T_0^{(0)}}{\mathrm{d}y}u + T_0^{(0)}\frac{\mathrm{d}^2w}{\mathrm{d}y^2}\frac{\mathrm{d}T_0^{(0)}}{\mathrm{d}y}\frac{\mathrm{d}w}{\mathrm{d}y} - \frac{4k^2}{3}T_0^{(0)}w, \quad \text{(B 10)}$$

and

$$h^* = T_0^{(0)}\frac{\mathrm{d}^2T}{\mathrm{d}y^2} + 2\frac{\mathrm{d}T_0^{(0)}}{\mathrm{d}y}\frac{\mathrm{d}T}{\mathrm{d}y} - \left[k^2T_0^{(0)} + \frac{1}{T_0^{(0)}}\left(\frac{\mathrm{d}T_0^{(0)}}{\mathrm{d}y}\right)^2\right]T. \quad \text{(B 11)}$$

REFERENCES

Albertoni, S., Cercignani, C. & Gotusso, L. 1963 Numerical evaluation of the slip coefficient. *Phys. Fluids* **6**, 993–996.

Aoki, K., Sone, Y. & Yoshimoto, M. 1999 Numerical analysis of the Taylor–Couette problem for a rarefied gas by the direct simulation Monte Carlo method. In *Rarefied Gas Dynamics* (eds R. Brun, R. Campragues, R. Gatignol & J. C. Lengrand), vol. 2, pp. 109–116. CÉPADUES, Toulouse.

Bird, G. 1981 Monte-Carlo simulation in an engineering context. In *Rarefied Gas Dynamics* (ed. S. S. Fisher). Progress in Astronantics and Aeronautics, vol. 74, pp. 239–255. AIAA.

Bird, G. 1994 *Molecular Gas Dynamics and the Direct Simulations of Gas Flows*. Clarendon Press.

Bird, G. A. 1998 Recent advances and current challenges for DSMC. *Comput. Math. Appl.* **35**, 1–14.

Cercignani, C. 2000 *Rarefied Gas Dynamics*. Cambridge University Press.

Chandrasekhar, S. 1961 *Hydrodynamic and Hydromagnetic Stability*. Clarendon Press.

Chapman, S. & Cowling, T. 1970 *The Mathematical Theory of Non-Uniform Gases*. 3rd edn. Cambridge University Press.

Drazin, P. & Reid, W. 1981 *Hydrodynamic Stability*. Cambridge University Press.

Epstein, A. H. 2004 Millimeter-scale, micro-electro-mechanical systems gas turbine engines. *Trans. ASME: J Engng Gas Turbines Power* **126**, 205–226.

Golshtein, E. & Elperin, T. 1995 Investigation of Bénard, Taylor and thermal stress instabilities in rarefied gases by direct simulation Monte Carlo method. *AIAA Paper* 95-2054.

Hatay, F. F., Biringen, S., Erlebacher, G. & Zorumski, W. E. 1993 Stability of high-speed compressible Couette flow. *Phys. Fluids* A **5**, 393–404.

Kao, K. & Chow, C. 1992 Linear stability of compressible Taylor–Couette flow. *Phys. Fluids* A **4**, 984–996.

Koschmieder, E. 1993 *Bénard Cells and Taylor Vortices*. Cambridge University Press.

Kuhlthau, A. R. 1960 Recent low-density experiments using cylinder techniques. *Rarefied gas Dynamics* (ed. F. M. Devienne), pp. 192–200. Pergamon.

Manela, A. & Frankel, I. 2005 On the Rayleigh–Bénard problem in the continuum limit. *Phys. Fluids* **17**, 036101.

Rayleigh, Lord 1916 On the dynamics of revolving fluids. *Sci. Pap.* **6**, 447–453.

Riechelmann, D. & Nanbu, K. 1993 Monte Carlo simulation of the Taylor instability in rarefied gas. *Phys. Fluids* A **5**, 2585–2587.

Sone, Y. 2002 *Kinetic Theory and Fluid Dynamics*. Birkhäuser.

Stefanov, S. & Cercignani, C. 1993 Monte Carlo simulation of the Taylor–Couette flow of a rarefied gas. *J. Fluid Mech.* **256**, 199–213.

Taylor, G. I. 1923 Stability of a viscous liquid contained between two rotating cylinders. *Phil. Trans. R. Soc.* A **223**, 289–343.

Usami, M. 1995 Direct simulation Monte Carlo on Taylor vortex flow. In *Rarefied Gas Dynamics* (ed. J. Harvey & G. Lord), vol. 1, pp. 389–395. Oxford University Press.

Yoshida, H. & Aoki, K. 2005 A numerical study of Taylor–Couette problem for a rarefied gas: Effect of rotation of the outer cylinder. In *Rarefied Gas Dynamics* (ed. M. Capitelli) American Institute of Physics, pp. 467–472.

Yoshida, H. & Aoki, K. 2006 Linear stability of the cylindrical Couette flow of a rarefied gas. *Phys. Rev.* E **73**, 021201.